Numerical and Experimental Study of a Plasma Actuator with Logarithmic Electrode Distribution

© V.V. Voevodin[1], Ya.E. Zharkov[1], O.I. Korzhova[1], G.M. Makaryants[2], V.Yu. Khomich[1], E.A. Shershunova[1], V.A. Yamshchikov[1]

[1] Institute for Electrophysics and Electric Power, Russian Academy of Sciences, St. Petersburg, Russia
[2] Samara National Research University, Samara, Russia
E-mail: yarik77794@mail.ru

Received April 30, 2025
Revised July 9, 2025
Accepted July 11, 2025

An analysis of the characteristics of a plasma actuator with a distributed tangential electric field has been performed. The generated thrust and energy efficiency were investigated experimentally and numerically for various waveform shapes of the applied voltage. Comparison with a classical configuration revealed increased thrust accompanied by a decrease in specific efficiency due to filament formation.

Keywords: surface dielectric barrier discharge, pulsed voltage, tangential electric field, electrohydrodynamics.

DOI: 10.61011/TPL.2025.12.62783.7966

Plasma actuators (PAs) are a promising means for controlling gas flow in the boundary layer by inducing volumetric electrodynamic forces [1]. Their advantages lie in the lack of moving parts, localization of impact, and high operation speed. The operation of most PAs is based on a surface dielectric barrier discharge (SDBD) that is initiated by applying voltage to an open electrode positioned on a dielectric barrier with a grounded substrate electrode on the opposite side [2]. Plasma channels forming along the surface of the barrier give rise to ion drift, which initiates electrohydrodynamic flow. Charge accumulation on the barrier surface leads to the formation of a counter electric field, which limits the discharge development [3].

The main PA characteristics are the gas flow velocity, the magnitude of induced thrust, and the energy efficiency, which is expressed through the specific thrust per unit of input power [4]. These characteristics are affected by the supply voltage parameters [5], the area of development of plasma channels, and the physical and electrical properties of the barrier material [6].

Three-electrode actuator designs, where an additional electrode forms a tangential electric field along the barrier, contributing to a more than 4-fold increase in induced thrust [8], were demonstrated to be efficient [7]. However, these designs require additional power sources, and their use is associated with the risk of interelectrode breakdown.

In the present study, we report the results of development of a PA with an electrode configuration that enhances the tangential electric field component. The key characteristics of the device, including the generated thrust and energy efficiency, were examined numerically and experimentally, and the obtained results were compared with the characteristics of a classical SDBD actuator.

The PA with an enhanced tangential field component was designed using a numerical model that is shown schematically in Fig. 1.

This model was used to solve the problem of maximizing the current of charged particles produced for variations of the geometric configuration of grounded electrodes located in the dielectric layer. The mathematical formulation of the problem for the model included a drift-diffusion equation for calculating the distribution of charged particle concentration $N(x, y, t)$ in electric field $V(x, y, t)$, which is characterized by the Poisson equation

$$\begin{aligned} &\mathrm{I}: \quad \nabla^2 V = \frac{-eN}{\varepsilon\varepsilon_0}, \\ &\mathrm{II}: \quad \frac{\partial N}{\partial t} = \nabla\left(\mu E(x, y)N - D\nabla N\right) = 0, \end{aligned} \tag{1}$$

where the relative permittivity of the dielectric substrate is $\varepsilon_r = 3.5$, particle mobility $\mu = 2.2 \cdot 10^{-4}\,\mathrm{m^2/(V \cdot s)}$, and diffusion coefficient $D = 5.6 \cdot 10^{-6}\,\mathrm{m^2/s}$. This approach to determining spatiotemporal distributions is used often in plasma applications due to its low computational complexity.

Fixed potential values were set at the electrode boundaries: $V_{HV}(t) = 10\,[\mathrm{kV}] \cdot \tanh(t \cdot 10^6\,[\mathrm{s^{-1}}])$ and zero potential were set at the high-voltage and grounded electrodes, respectively. Charging of the dielectric surface (Fig. 1, quantity σ) was taken into account through the balance of the normal current component defined by the scalar product of charged particle flux Γ_N and surface normal n. When the critical voltage at the active electrode with rounding radius r was exceeded, charge sources were introduced into the transport equation with the use of a variational constraint based on Lagrange multipliers.

The geometric configuration of grounded electrodes was varied with the aim of maximizing the current through the use of fourth-order Bernstein polynomials. The optimization

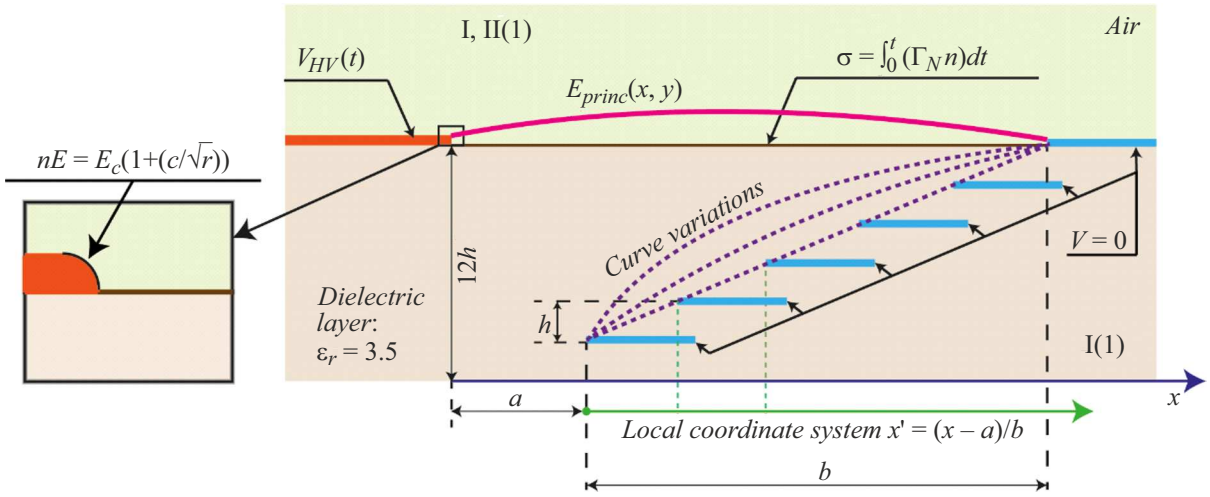

Figure 1. Schematic diagram of the actuator and key parameters for optimizing its design.

problem itself was formulated as

$$x = \arg\max \int_{\Omega_{air}} e\Gamma_N(t_{1c}, x)d\Omega_{air}, \quad x = \left[b, a, x_{el}\right]^T,$$

$$x_{el,i} = a + b\sum_{k=0}^{n} \beta_k z_{k,n}\left(\frac{i}{9}\right), \quad \beta_k \in \mathbb{R}^n,$$

$$z_{k,n}(x') = \binom{n}{k} x'^k (1-x')^{n-k}, \quad x' \in [0,\ 1], \qquad (2)$$

where e is the elementary charge, β_k are the polynomial coefficients, x' is the normalized coordinate, a is the width of the gap between grounded electrodes and the surface electrode, and b is the width of the region where the grounded electrodes are located. To avoid a trivial solution to problem (2), additional restrictions imposed on the Townsend criterion were applied:

$$K > \ln\left(1 + \frac{1}{\gamma}\right), K < 17.7 + \ln\left(\frac{l}{1[\text{cm}]}\right),$$

$$K = \int_0^l \alpha_{eff} E_{princ}(s)ds, \qquad (3)$$

where γ is the secondary emission coefficient (0.07); l is the length of the field line; α_{eff} is the effective impact ionization coefficient [9]; and $E_{princ}(s)$ is the field strength along the principal line. The optimization procedure was implemented using MATLAB for iterative optimization and a software package with a finite element solver.

Figure 2, *a* presents the geometric configuration of the optimized PA (TF-PA), where the logarithmically approximated distribution of grounded electrodes is the result of numerical optimization. The results of numerical simulation of a discharge without the surface charge performed for optimized and classical plasma actuator designs are shown in the same figure. The aim of the numerical study was to conduct a comparative analysis of the integral characteristics of actuators (see Figs. 2, *b*, *c*): the high-voltage electrode current and the magnitude of instantaneous Coulomb forces. Modeling was carried out for air using a hydrodynamic model in the approximation of average electron energy at a positive voltage polarity (8 kV). The reaction scheme included impact ionization, attachment, and excitation of N_2 and O_2 molecules with equivalent energy losses [9]. The excitations of N_2 singlet states with an optical transition ($\lambda \approx 100$ nm), the relaxation of which formed a photoionization source in a model based on the SP_3 approximation of the radiative heat conduction equation, were taken into account. The finite element mesh was triangular with a size of 1 μm at the interface and 3 μm in the bulk down to 100 μm.

The potential distributions shown in Fig. 2 make it clear that a longitudinal gradient of ~ 7.8 kV/cm forms along the streamer body in the optimized (TF-PA) actuator configuration; in the classical (SDBD) configuration, the SDBD channel remains virtually equipotential. This field profile is indicative of increased channel conductivity and enhanced longitudinal current in the developed design. The calculated waveforms (Fig. 2, *b*) confirm this: the peak discharge current value for the optimized actuator is almost 5 times higher. This increase is attributable to a combination of a greater capacitive component and the contribution of conduction current in the streamer channel. Figure 2 presents the instantaneous values of generated thrust; the maximum value obtained in the developed configuration is 17 times higher than the corresponding maximum in the design with a classical SDBD.

To validate the calculated data, PAs of both (optimized and classical) designs (Fig. 2, *a*; active zone length, 6 cm) and an experimental circuit (Fig. 3) for recording the values of power consumed by the discharge and the generated thrust were constructed. The experimental setup

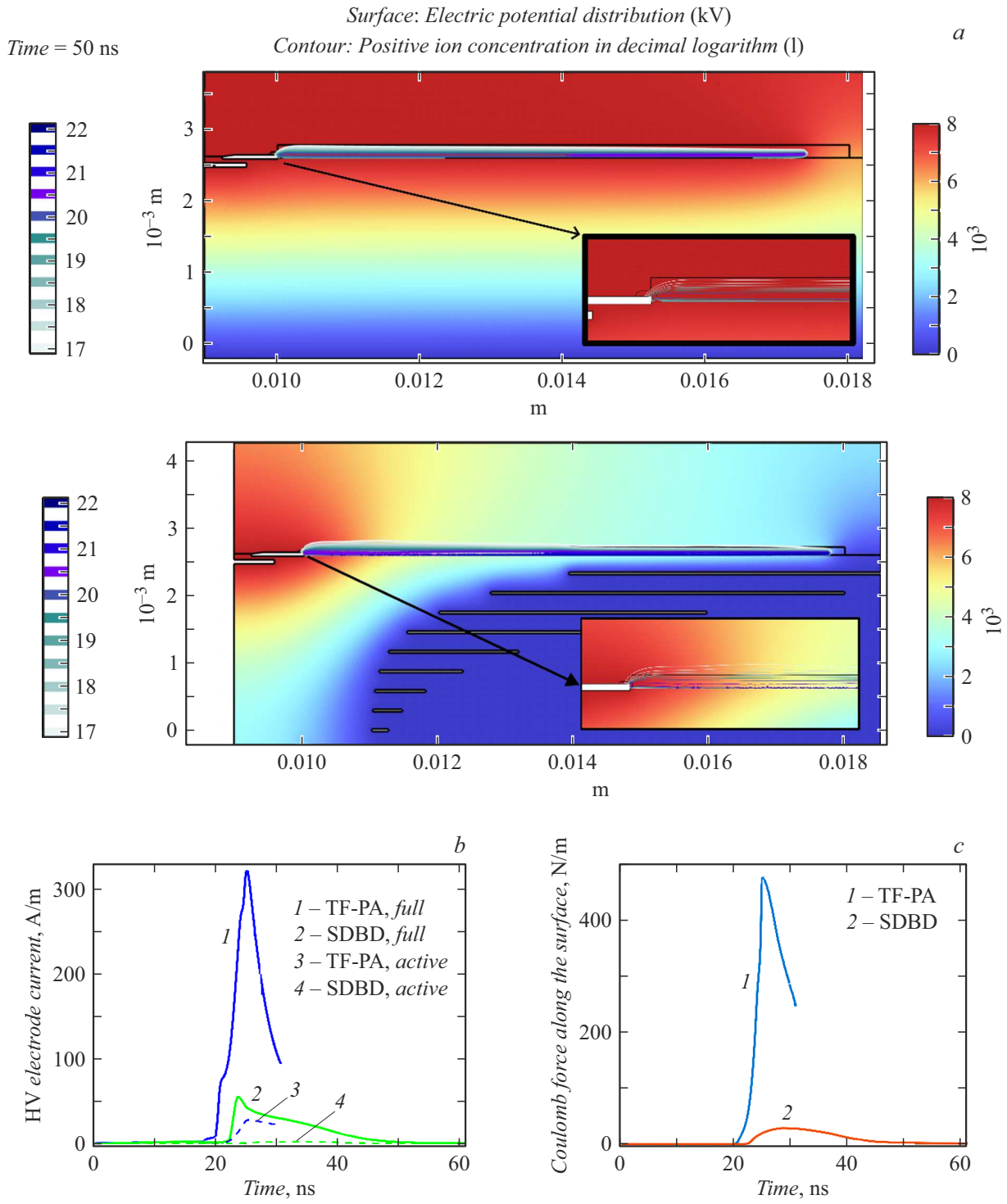

Figure 2. *a* — results of numerical simulation of a discharge in the classical (SDBD) (upper image) and optimized (TF-PA) (lower image) PA geometries; *b* — components of the total and active actuator current; *c* — instantaneous thrust values integrated over the volume.

included power sources producing sawtooth and meander voltage pulses with a frequency of 10 kHz [10,11]; an OHAUS STX123 scale (1 mg accuracy) for thrust recording; capacitor $C_{meas} = 80$ nF and a Tektronix P6015A (u_{reg}) high-voltage probe for measuring the discharge power; and a Canon EOS 6D Mark II camera (90 pix/mm; exposure time, 0.5 s; ISO 100) for monitoring the discharge structure.

The experimental results are presented in Fig. 4. The voltage dependence of the generated thrust (Fig. 4, *a*) matches the data obtained at NASA Langley Research Center [5]:

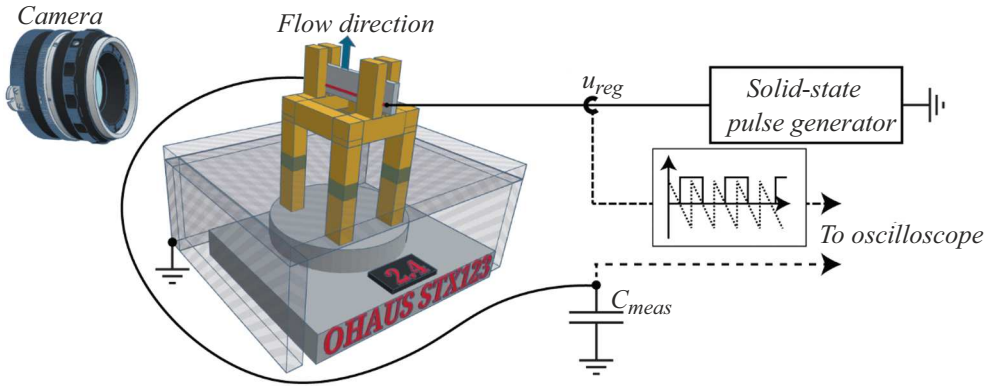

Figure 3. Diagram of the experimental setup for recording the thrust and power characteristics of a discharge.

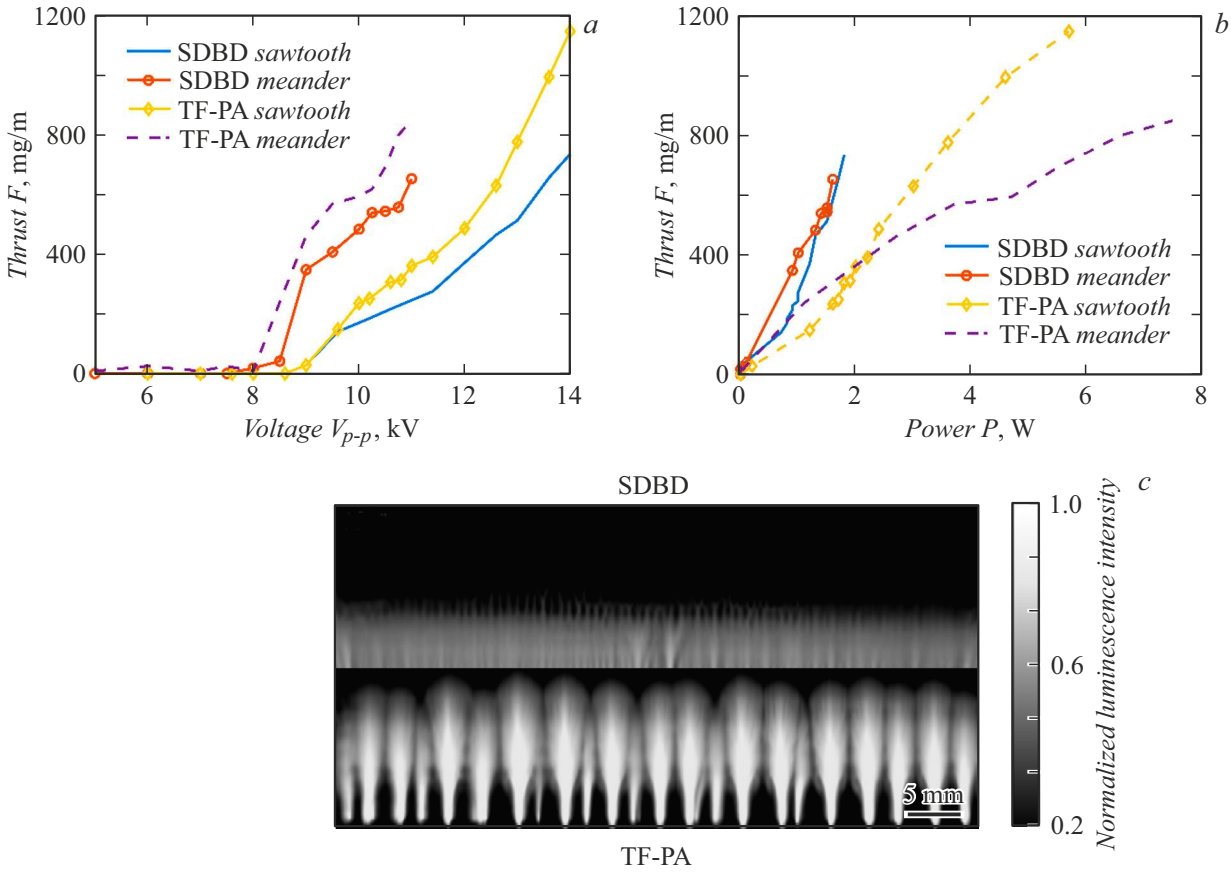

Figure 4. Experimental dependences of thrust F on peak-to-peak amplitude V_{p-p} of voltage pulses (a) and discharge power P (b); recorded discharge structure and normalized glow intensity (c) at a supply voltage (meander) of -11 kV.

at equal amplitude voltages, a meander signal provides a twofold increase in thrust compared to a sawtooth one. The optimized electrode configuration provides a further 25–30 % increase in thrust compared to a conventional SDBD actuator.

The dependence of thrust on input power (Fig. 4, b) reveals a 2-fold reduction in energy efficiency of the new design (compared to the SDBD). To analyze the causes of this, we compared the discharge structures and the distributions of normalized optical brightness in the blue spectral range (Fig. 4, c).

According to Fig. 4, c, a filamentary discharge structure forms in the developed design [12], which is indicative of an increase in conduction current and active heat release. The glow is brighter due to an increase in electrical power. This was also confirmed indirectly by numerical modeling.

Thus, the results of numerical and experimental studies demonstrate the advantage of the proposed actuator

configuration in generated thrust, but also suggest that further optimization through the adjustment of forms and parameters of the supply voltage or materials of the active electrode is needed in order to reduce the losses associated with the formation of a filamentary discharge.

Funding

This study was supported financially by the Ministry of Science and Higher Education of the Russian Federation (grant for major research projects in priority areas of scientific and technological development, agreement No. 075-15-2024-558).

Conflict of interest

The authors declare that they have no conflict of interest.

References

[1] K. Iranshahi, T. Defraeye, R.M. Rossi, U.C. Müller, Int. J. Heat Mass Transfer, **232**, 125895 (2024). DOI: 10.1016/j.ijheatmasstransfer.2024.125895
[2] T.C. Corke, M.L. Post, D.M. Orlov, Exp. Fluids, **46**, 1 (2009). DOI: 10.1007/s00348-008-0582-5
[3] A. Houpt, S.B. Leonov, J. Appl. Math. Phys., **3** (8), 1062 (2015). DOI: 10.4236/jamp.2015.38132
[4] M. Kotsonis, Meas. Sci. Technol., **26**, 092001 (2015). DOI: 10.1088/0957-0233/26/9/092001
[5] D.F. Opaits, *Dielectric barrier discharge plasma actuator for flow control (NASA/CR-2012-217655)*, NASA technical reports (Princeton University, 2012).
[6] J. Pons, E. Moreau, G. Touchard, J. Phys. D, **38**, 3635 (2005). DOI: 10.1088/0022-3727/38/19/012
[7] S. Sato, K. Mitsuhashi, T. Enokido, A. Komuro, A. Ando, N. Ohnishi, J. Phys. D, **54**, 455203 (2021). DOI: 10.1088/1361-6463/aca61d
[8] S. Sato, M. Sakurai, N. Ohnishi, J. Appl. Phys., **132**, 113301 (2022). DOI: 10.1063/5.0100696
[9] *Phelps and IAA electron collision cross-section databases, LXCat: Open-Access Database for Electron Transport and Scattering* [Electronic source]. www.lxcat.net
[10] V.Yu. Khomich, S.I. Moshkunov, A.B. Prokofiev, E.A. Shershunova, Acta Astron., **225**, 99 (2024). DOI: 10.1016/j.actaastro.2024.09.008
[11] Ya.E. Zharkov, S.I. Moshkunov, I.E. Rebrov, V.Yu. Khomich, V.A. Yamshchikov, Instrum. Exp. Tech., **65** (4), 593 (2022). DOI: 10.1134/S002044122204025X.
[12] S.A. Stepanyan, A.Y. Starikovskiy, N.A. Popov, S.M. Starikovskaia, Plasma Sources Sci. Technol., **23** (4), 045003 (2014). DOI: 10.1088/0963-0252/23/4/045003

Translated by D.Safin